

# Electromagnetically induced grating: Homogeneously broadened medium

Hong Yuan Ling

*Department of Chemistry and Physics, Rowan University, Glassboro, New Jersey 08028*

Yong-Qing Li and Min Xiao

*Department of Physics, University of Arkansas, Fayetteville, Arkansas 72701*

(Received 14 April 1997; revised manuscript received 10 September 1997)

A strong coupling standing wave, interacting with three-level  $\Lambda$ -type (or ladder-type) atoms, can diffract a weak probe field (propagating along a direction normal to the standing wave) into high-order diffractions, a phenomenon which we name electromagnetically induced grating (EIG). We develop in this work a theory for studying EIG in a homogeneously broadened medium consisting of three-level  $\Lambda$ -type atoms. We show that by taking advantage of the absorption and dispersion properties of electromagnetically induced transparency one can create an atomic grating that can effectively diffract light into the first-order direction. [S1050-2947(98)03902-X]

PACS number(s): 42.50.Gy, 42.50.Hz, 42.65.An

## I. INTRODUCTION

It is commonly believed that a weak probe beam will be strongly absorbed at its resonance frequency if most of the atoms are in the lower level. However, recent studies show that by coupling additional coherent fields with other atomic transitions, one can form coherent population trapping (CPT) [1,2] states that render a medium transparent to the weak probe radiation. This phenomenon is known as electromagnetically induced transparency (EIT) [3–5]. CPT and EIT are the principal mechanisms behind many recent applications, such as lasing without population inversion [6–12], enhancement of second- and third-order nonlinear processes [13–15], velocity selective laser cooling [16–18], atomic mirrors [19–20], matching pulses [21,22], electromagnetically induced focusing [23], and elimination of optical self-focusing [24]. In this paper we explore a new possibility of their application: electromagnetically induced grating (EIG).

Consider a system as shown in Fig. 1(a). It consists of two strong coupling fields of frequency  $\omega_c$  and wave number  $k_c$ , a weak probe field of frequency  $\omega_p$  and wave number  $k_p$ , and an atomic sample. The atomic sample hosts three-level  $\Lambda$ -type (or ladder-type) atoms whose energy diagram is shown in Fig. 1(b). As usual, the coupling fields drive the  $2 \leftrightarrow 3$  atomic transition (which has a transition frequency  $\Omega_{23}$  and a dipole moment  $\mu_{23}$ ), while the probe field induces the  $2 \leftrightarrow 1$  atomic transition (which has a transition frequency  $\Omega_{21}$  and a dipole moment  $\mu_{21}$ ); the  $3 \leftrightarrow 1$  atomic transition is a dipole forbidden one. Here, the two coupling fields, while being symmetrically displaced with respect to  $z$ , are incident upon the atomic sample at such angles that they intersect and form a standing wave inside the medium. Because of the weak nature of the probe field, levels 2 and 3 remain virtually empty no matter what the intensities of the coupling fields are. As a result, the standing wave has an amplitude and space period that are immune to the interaction of light with the atoms. Since the absorption and dispersion coefficients of the probe field depend on the strength of the coupling fields, they are expected to change periodically as the standing wave changes from nodes to antinodes across  $x$

dimension. Such a medium will exert both amplitude and phase modulations across the probe beam profile in much the same way that a hybrid (amplitude and phase) grating does to the amplitude and phase of an electromagnetic wave. We name this phenomenon EIG.

The principal mechanism behind EIG is EIT. To illustrate this point, we compare in Fig. 2 the absorption and dispersion in the absence of the coupling field (dashed curves) with the ones in the presence of a strong resonant coupling field (solid curves). We further assume that the intensity of the coupling field (used for producing the solid curve in Fig. 2) corresponds to the peak intensity of a standing wave. Then, the dashed curves are what the probe field at nodes “sees,” and the solid curves are what the probe field at antinodes “sees.” The medium within the EIT window, while being quite opaque to the probe field at nodes, is almost transparent to the probe fields at antinodes as shown in Fig. 2(a). This

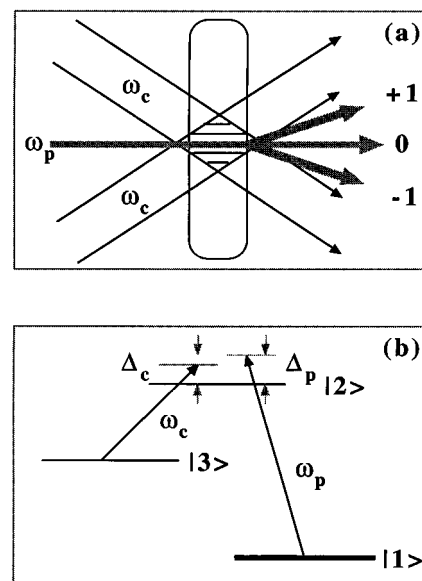


FIG. 1. (a) A sketch of a prototype experimental setup. (b) The energy diagram of three-level  $\Lambda$ -type atoms.

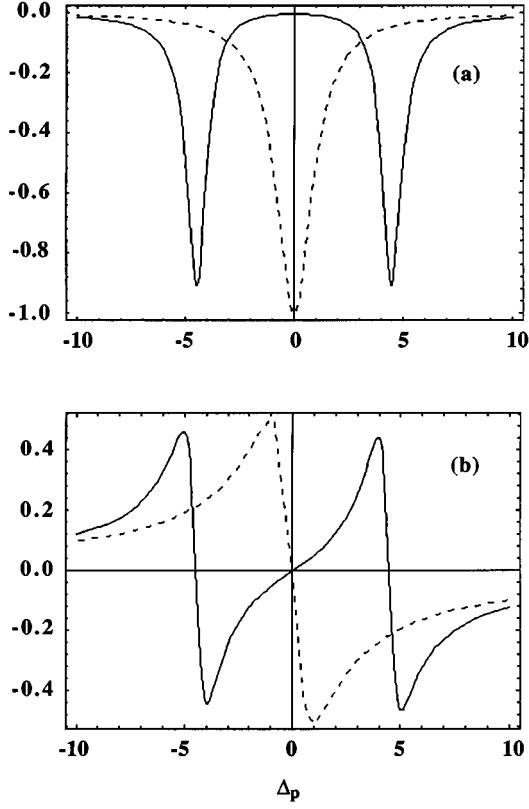


FIG. 2. (a) Absorption spectrum and (b) dispersion spectrum. The dashed curves are produced without the coupling field. The solid ones are produced with a strong resonant coupling field. The units and parameters are arbitrary.

can lead to a substantial amplitude modulation across the probe beam. The dispersion within the EIT window is positive to the probe field at nodes but negative to the probe field at antinodes, or vice versa [Fig. 2(b)]. This opens the possibility of a large phase modulation across the probe beam.

In what follows, we present a theoretical analysis of EIG, and show how these novel properties within the EIT window can be utilized to produce an atomic grating that can effectively diffract light into the first-order direction.

## II. THEORETICAL MODEL

Our analysis begins with the mathematical representations for the electromagnetic fields inside the medium. The probe field is expressed as

$$F_p(x, z, t) = \frac{1}{2} F_p e^{-i\omega_p t + ik_p z} + \text{c.c.}, \quad (1)$$

where  $F_p$  is a slowly varying function of time  $t$  and distance  $z$ , and c.c. stands for complex conjugate operation. The two coupling fields have wave vectors that are composed of an  $x$  component  $k_{cx}$  (or  $-k_{cx}$ ) and a  $z$  component  $k_{cz}$ , where  $k_{cx}^2 + k_{cz}^2 = k_c^2$ . They form, in the overlap region, a standing wave (along  $x$  dimension) with a mathematical expression

$$F_c(x, z, t) = \frac{1}{2} F_c \sin(\pi x / \Lambda_{cx}) e^{-i\omega_c t + ik_{cz} z} + \text{c.c.}, \quad (2)$$

where  $F_c$  is assumed to be a real constant for simplicity, and  $\Lambda_{cx} (= \pi / k_{cx})$  represents the space period.  $\Lambda_{cx}$  can be made arbitrarily larger than the wavelength of the coupling fields

by varying the angle between the two wave vectors of the corresponding coupling fields. The response of the medium to the fields is governed by the density-matrix equation, which, in the interaction picture, takes the form

$$\frac{\partial \rho'}{\partial t} = -\frac{i}{\hbar} [H'_I, \rho'] + \Lambda \rho', \quad (3)$$

where  $\rho'$  stands for the density-matrix operator,  $\Lambda \rho'$  summarizes the effects due to the interaction of atoms with random fluctuations, and  $H'_I$  is the interaction Hamiltonian. In the Hilbert space spanned by the bare states ( $|1\rangle, |2\rangle, |3\rangle$ ) and under the rotational wave approximation,  $H'_I$  can be represented by

$$H'_I = -\hbar \{ [E_p e^{-i\Delta_p t + ik_p z} |2\rangle \langle 1| + E_c \sin(\pi x / \Lambda_{cx}) e^{-i\Delta_c t + ik_{cz} z} |2\rangle \langle 3|] + \text{c.c.} \}, \quad (4)$$

where

$$E_p = \frac{1}{2} \frac{\mu_{21} F_p}{\hbar}, \quad E_c = \frac{1}{2} \frac{\mu_{23} F_c}{\hbar} \quad (5)$$

are the Rabi frequencies of the corresponding fields, and  $\Delta_p (= \omega_p - \Omega_{21})$  and  $\Delta_c (= \omega_c - \Omega_{23})$  are the frequency detunings of probe and coupling fields. By expanding Eq. (3) in terms of the newly defined density-matrix elements

$$\rho_{21} = \rho'_{21} e^{i\Delta_p t - ik_p z}, \quad \rho_{23} = e^{i\Delta_c t - ik_{cz} z} \rho'_{23}, \quad (6)$$

$$\rho_{31} = e^{i(\Delta_p - \Delta_c)t - i(k_p - k_{cz})z} \rho'_{31}, \quad \rho_{ii} = \rho'_{ii},$$

we can easily arrive at their equations of motion:

$$\frac{\partial \rho_{11}}{\partial t} = \Gamma_{21} \rho_{22} + \Gamma_{31} \rho_{33} + iE_p^* \rho_{21} - iE_p \rho_{12}, \quad (7a)$$

$$\begin{aligned} \frac{\partial \rho_{33}}{\partial t} = & \Gamma_{23} \rho_{22} - \Gamma_{31} \rho_{33} + iE_c \sin(\pi x / \Lambda_{cx}) \rho_{23} \\ & - iE_c \sin(\pi x / \Lambda_{cx}) \rho_{32}, \end{aligned} \quad (7b)$$

$$\begin{aligned} \frac{\partial \rho_{21}}{\partial t} = & (-\gamma_{21} + i\Delta_p) \rho_{23} + iE_p (\rho_{11} - \rho_{22}) \\ & + iE_c \sin(\pi x / \Lambda_{cx}) \rho_{31}, \end{aligned} \quad (7c)$$

$$\begin{aligned} \frac{\partial \rho_{23}}{\partial t} = & (-\gamma_{23} + i\Delta_p) \rho_{23} + iE_p \rho_{13} \\ & + iE_c \sin(\pi x / \Lambda_{cx}) (\rho_{33} - \rho_{22}), \end{aligned} \quad (7d)$$

$$\begin{aligned} \frac{\partial \rho_{31}}{\partial t} = & [-\gamma_{31} + i(\Delta_p - \Delta_c)] \rho_{31} \\ & + iE_c \sin(\pi x / \Lambda_{cx}) \rho_{21} - iE_p \rho_{32}, \end{aligned} \quad (7e)$$

$$\rho_{ij} = (\rho_{ji})^*, \quad i \neq j, \quad (7f)$$

$$\rho_{11} + \rho_{22} + \rho_{33} = 1, \quad (7g)$$

where  $\Gamma_{ij}$  is the population decay rate from levels  $i$  to  $j$  while  $\gamma_{ij}$  is the dephasing rate between levels  $i$  and  $j$ . In deriving Eq. (7), the atomic system has been assumed to be closed. The interaction of atoms with fields induces a polarization that oscillates at the frequency of the weak probe field:

$$P_p(x, z, t) = \frac{1}{2} P_p e^{-i\omega_p t + ik_p z} + \text{c.c.}, \quad (8)$$

where  $P_p$  is the slowly varying polarization. By performing a quantum average of the dipole moment over an ensemble of homogeneously broadened atoms, we find

$$P_p = 2N\mu_{12}\rho_{21}, \quad (9)$$

where  $N$  is the atomic density. This polarization becomes the term on the right side of Maxwell's equation for the probe field, which reduces to

$$-i \frac{1}{2k_p} \frac{\partial^2 F_p}{\partial x^2} + \frac{\partial F_p}{\partial z} = i \frac{k_p}{2\epsilon_0} P_p, \quad (10)$$

under the slowly varying amplitude approximation and in steady state. To obtain a self-consistent equation for  $E_p$ , we

first follow the method in Ref. [25] to obtain, from Eq. (7), a solution to  $\rho_{21}$  correct to all orders of the coupling field, but linear order of the weak probe. We then substitute this  $\rho_{21}$  into Eq. (9), and replace  $P_p$  in Eq. (10) with the newly derived expression. To present the results in a unitless form, we choose  $\gamma_{21}$  as the unit for all the decay rates, frequency detunings, and Rabi frequencies,  $\Lambda_{cx}$  as the unit for  $x$ , and  $z_0$  as the unit for  $z$ , where

$$z_0 = \frac{2\hbar\gamma_{21}\epsilon_0}{Nk_p\mu_{21}^2} \quad (11)$$

is the resonant (amplitude) absorption distance at  $e^{-1}$  in the absence of the coupling fields. Finally, the wave equation for the probe field, in a self-consistent and unitless form, becomes

$$-i \frac{1}{N_F} \frac{\partial^2 E_p}{\partial x^2} + \frac{\partial E_p}{\partial z} = (\alpha_r + i\alpha_i) E_p, \quad (12)$$

where

$$\alpha_r(x) = - \frac{[\gamma_{31}^2 + (\Delta_p - \Delta_c)^2] + \gamma_{31} I_c \sin^2(\pi x)}{(1 + \Delta_p^2)[\gamma_{31}^2 + (\Delta_p - \Delta_c)^2] + 2[\gamma_{31} - \Delta_p(\Delta_p - \Delta_c)]I_c \sin^2(\pi x) + I_c^2 \sin^4(\pi x)}, \quad (13)$$

$$\alpha_i(x) = \frac{-\Delta_p[\gamma_{31}^2 + (\Delta_p - \Delta_c)^2] + (\Delta_p - \Delta_c)I_c \sin^2(\pi x)}{(1 + \Delta_p^2)[\gamma_{31}^2 + (\Delta_p - \Delta_c)^2] + 2[\gamma_{31} - \Delta_p(\Delta_p - \Delta_c)]I_c \sin^2(\pi x) + I_c^2 \sin^4(\pi x)}, \quad (14)$$

with

$$I_c = E_c^2,$$

are the absorption and dispersion coefficients of the probe field, and

$$N_F = \frac{(2\sqrt{\pi}\Lambda_{cx})^2}{\lambda_p z_0} \quad (15)$$

is the Fresnel number of a slit of a width  $2\sqrt{\pi}\Lambda_{cx}$  at a distance  $z_0$ . Note that since no ambiguity is likely to occur the same symbols are used for the scaled variables. The transverse term (the second-order derivative of the field with respect to  $x$ ) in Eq. (12) makes the probe field nonlocal in the sense that the field at  $x$  will affect the field at different  $x$  as it propagates along  $z$  inside the medium. This will complicate the interpretation of the physics involved in the EIG formation. In this work, to focus on the main features of EIG, we eliminate the transverse term by working in a parameter regime where  $N_F \gg 1$ . Such a requirement can be realized by increasing atomic density or  $\Lambda_{cx}$ . Under this condition, Eq. (12) can be solved analytically to obtain the transmission function for a medium of thickness  $L$  (along  $z$ ):

$$T(x) = e^{\alpha_r(x)L} e^{i\alpha_i(x)L}. \quad (16)$$

The far-field distribution (Fraunhofer diffraction) over the diffraction angle  $\theta$  (with respect to  $z$  direction) is proportional to the Fourier transformation of the product of the input probe field amplitude  $E_0(x)$  and the transmission function:

$$E_p(\theta) = C \int_{-\infty}^{+\infty} E_0(x) T(x) \exp(-i2\pi\Lambda_{cx}x \sin\theta/\lambda_p) dx, \quad (17)$$

where  $C$  is the proportionality. Assuming the input probe field is a plane wave having an amplitude  $E_0$  uniform across a beam of a width of  $N$  times  $\Lambda_{cx}$  and defining  $I_p(\theta)$  as  $|E_p(\theta)|^2$  normalized to  $(CE_0N)^2$ , we find from Eq. (17) that

$$I_p(\theta) = |E_p^1(\theta)|^2 \frac{\sin^2(N\pi\Lambda_{cx}\sin\theta/\lambda_p)}{N^2\sin^2(\pi\Lambda_{cx}\sin\theta/\lambda_p)}, \quad (18)$$

where

$$E_p^1(\theta) = \int_0^1 T(x) \exp(-i2\pi\Lambda_{cx}x \sin\theta/\lambda_p) dx \quad (19)$$

represents the Fraunhofer diffraction of a single space period. Since we will be mainly interested in the first-order

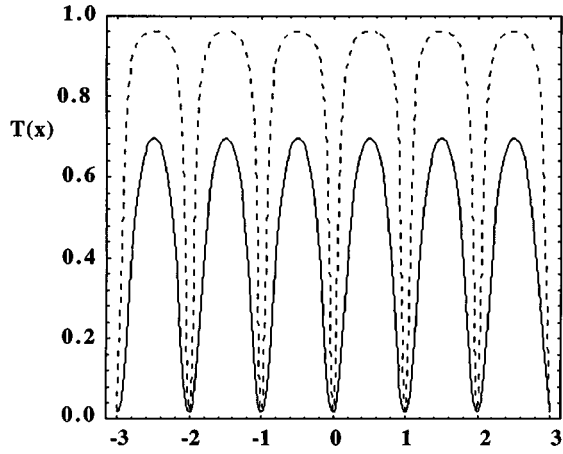


FIG. 3. The transmission function as a function of  $x$  when both  $\Delta_c$  and  $\Delta_p$  are zero, and  $I_c=2.0$  (solid curve) and 10 (dashed curve). Other parameters are  $\gamma_{31}=0.1$ , and  $L=4$ .

diffraction, we calculate  $I_p(\theta)$  along the first-order diffraction angle determined by the grating equation,  $\sin\theta_1 = \lambda_p/\Lambda_{cx}$ , with the result

$$I_p(\theta_1) = |E_p^1(\theta_1)|^2, \quad (20)$$

where

$$E_p^1(\theta_1) = \int_0^1 T(x) \exp(-i2\pi x) dx. \quad (21)$$

### III. RESULTS AND DISCUSSIONS

In this section, the equations outlined in Sec. II are used to investigate the diffraction power of the EIG under various parameters. Let us begin our study with a case in which both  $\Delta_p$  and  $\Delta_c$  are zero. A simple inspection of Eq. (14) reveals that  $\alpha_i$  vanishes, implying that no phase modulation takes place. The transmission function [Eq. (16)] is therefore simplified to  $\exp(\alpha_r L)$ , where

$$\alpha_r = -\frac{1}{1 + I_c/\gamma_{31}\sin^2(\pi x)}. \quad (22)$$

Figure 3 displays two typical transmission functions. The two curves share all the parameters except  $I_c$ ; the  $I_c$  for the dashed curve is ten times as large as the one for the solid one. At the transverse locations around the nodes (of the standing wave), the coupling field intensity is very weak, and the probe field is absorbed according to the usual Beer law. In contrast, at the transverse locations around the antinodes, the coupling field intensity is quite strong, and the probe field is absorbed much less because of the EIT. This leads to a periodic amplitude modulation across the beam profile of the probe field, a phenomenon reminiscent of the amplitude grating. Figure 4 displays the corresponding Fraunhofer diffraction patterns. To illustrate the efficiency of the first-order diffraction of this grating, we use Eq. (20) to calculate  $I_p(\theta_1)$  and display the result as a function of  $I_c/\gamma_{31}$  in Fig. 5. At small  $I_c$ , it increases almost linearly with  $I_c$ . This is within our expectation because as  $I_c$  increases, EIT will gradually open up the individual antinodes, making more light avail-

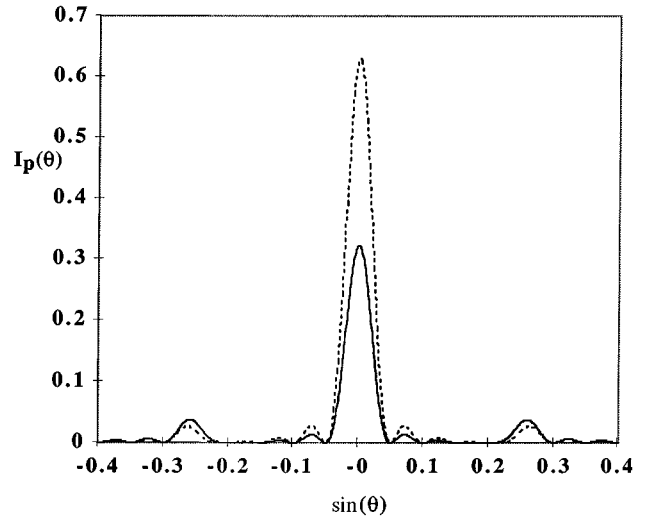


FIG. 4. The normalized diffraction intensity  $I_p(\theta)$  as a function of  $\sin(\theta)$  when both  $\Delta_c$  and  $\Delta_p$  are zero, and  $I_c=2$  (solid curve) and 10 (dashed curve). Other parameters are  $\gamma_{31}=0.1$ ,  $L=4$ ,  $\Lambda_{cx}/\lambda_p=4$ , and  $N=5$ .

able for diffraction into the first order. However, it peaks at a certain  $I_c$ , beyond which it fades away. This seemingly contradictory effect can be resolved by the following consideration. A strong coupling field can render most of a single period of the grating transparent, as clearly demonstrated by the dashed curve in Fig. 2. Such a wide opening single period is known to possess a diffraction envelope highly concentrated along the forward direction, limiting the chances of light to stray into the first order. This explains why the dashed curve in Fig. 4, while it enjoys a much increased center maximum, has a weaker first-order peak (around  $\sin\theta=0.25$ ) compared to the solid curve. In summary, the first-order diffraction attainable by this pure amplitude grating is very limited.

To increase the efficiency of the first-order diffraction, we must move into a parameter regime where the phase modulation is significant. Ideally, we wish to create a medium that is completely transparent to the probe field, but has a phase

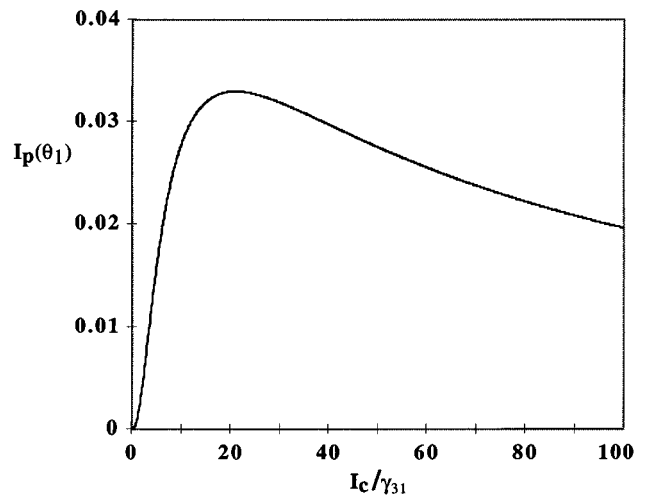


FIG. 5. The normalized first-order diffraction intensity  $I_p(\theta_1)$  as a function of  $I_c/\gamma_{31}$  when both  $\Delta_c$  and  $\Delta_p$  are zero, and  $L=4$ .

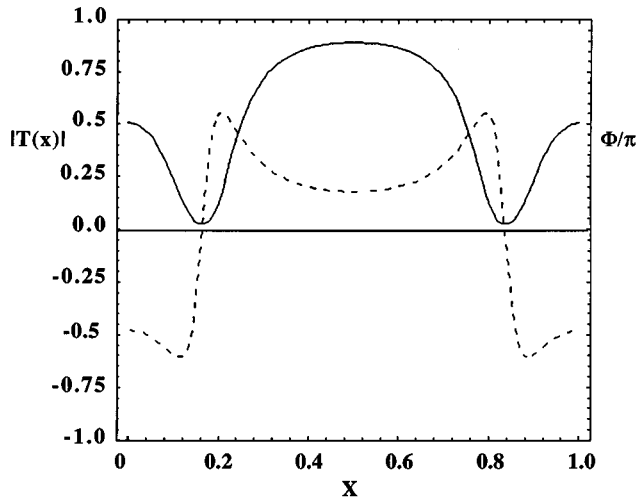


FIG. 6. The amplitude of the transmission function  $|T(x)|$  (solid curve) and the phase of the transmission function  $\Phi$  (dashed curve) as a function of  $x$  within a single space period when  $\gamma_{31}=0.1$ ,  $L=4$ ,  $\Delta_c=2.2$ , and  $I_c=20$ .

modulation on the order of  $\pi$  across the probe beam. The diffraction power of a phase grating plus the fact that no loss of energy takes place inside the medium makes such a grating highly efficient in diffracting light into high-order directions. Although it is impossible to realize this ideal grating in our model, we will be in search of parameters that can yield a grating as close as possible to the ideal one. In light of this discussion, we decide to work in a parameter regime where the coupling fields have a high intensity and are on resonance with the  $2 \leftrightarrow 3$  transition, but the weak probe is tuned away from the  $2 \leftrightarrow 1$  transition but still operates within the EIT window. The former condition is aimed to keep a good level of transparency across the beam profile while the latter one is designed to introduce a nonzero  $\alpha_i$  [Eq. (14)], therefore, a phase modulation of the probe field. Figure 6 displays, over a single period, the absorption  $|T(x)|$  (solid curve) and phase  $\Phi (= \alpha_i L)$  (dashed curve) produced when

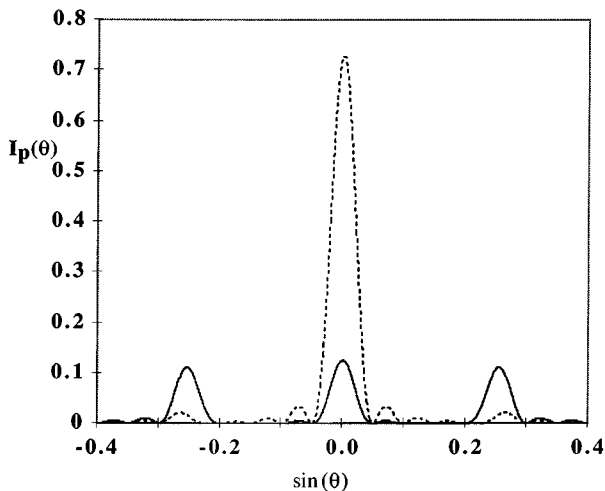


FIG. 7. The normalized diffraction intensity  $I_p(\theta)$  as a function of  $\sin(\theta)$  when  $\Delta_p=0$  (dashed curve) and 2.2 (solid curve). Other parameters are  $\gamma_{31}=0.1$ ,  $L=4$ ,  $\Delta_c=0$ ,  $I_c=20$ ,  $\Lambda_{cx}/\lambda_p=4$ , and  $N=5$ .

$I_c=20$  and  $\Delta_p=2.2$ . In this figure, the nodes are located on both ends of the curves while the antinode is located in the middle. At nodes, both absorption and dispersion are about 0.5 (far from zero) because the probe is tuned away from resonance. The maximum absorptions are reached at locations where the probe detuning matches the Rabi sideband, that is,  $I_c \sin^2(\pi x) = \Delta_p^2$ , which yields two  $x$  values: 0.16 and 0.84. Both the absorption and phase experience a rapid change around  $x=0.16$  and 0.84, but remain relatively flat around the antinode. These curves, although far from ideal, bear some traits of the ideal phase grating. First, the absorption is close to one across most of the single period. Second, the difference between the minimum and maximum phases is on the order of  $\pi$ . Figure 7 compares the diffraction pattern in this case where  $\Delta_p$  is 2.2 (solid curve) with the one where  $\Delta_p$  is zero (dashed curve) (other parameters are the same). It shows that the amount of light in the first order is, as we predict, considerably increased. To illustrate the role of the phase modulation, we present in Fig. 8 two figures; one is the Fraunhofer diffraction of  $|T(x)|$  (solid curve), and the other is the Fraunhofer diffraction of  $\exp(i\Phi)$  (dashed curve). It clearly shows that the amplitude modulation tends to gather light to the center maximum while the phase modulation tends to disperse light into the high-order directions. Therefore we conclude that the transfer of light from the center maximum to the first order, demonstrated by the solid curve in Fig. 7, is mainly accomplished by the phase modulation. The next question is how far  $\Delta_p$  should be detuned in order to yield an optimum first-order diffraction. Figure 9 is produced to answer this question. It shows that the first-order diffraction increases as  $\Delta_p$  until it reaches a maximum value, beyond which it decreases as  $\Delta_p$ . When  $\Delta_p$  is too large, the diffraction power is reduced because a large  $\Delta_p$ , although it makes the medium more transparent, weakens the key diffraction player: dispersion.

#### IV. CONCLUSION

In this paper we have developed a theory for studying the phenomenon of electromagnetically induced grating in a homogeneously broadened medium consisting of three-level  $\Lambda$ -type atoms under the condition that  $N_F \gg 1$  [Eq. (15)]. We have used this theory to investigate the transmission function of the medium and the Fraunhofer diffraction of the probe field when both coupling and probe fields are on resonance with their corresponding atomic transitions. We find that the atomic medium under this condition serves as an amplitude grating to the probe field with a very limited diffraction power. This is because a strong coupling field renders most of a single period of this grating transparent. Such a single period creates a diffraction envelope that is highly concentrated along the forward direction, leaving very little opportunity for light to propagate along the first-order direction. We have also investigated the transmission function and the diffraction power of the medium in the parameter regime where the probe frequency is tuned away from resonance (but still within the EIT window) and the coupling field intensity remains high. A high  $I_c$  reduces the loss of light, while a nonzero  $\Delta_p$  introduces a periodic phase modulation across the probe beam. We find that this scheme takes advantage of the two features of EIT: transparency and high

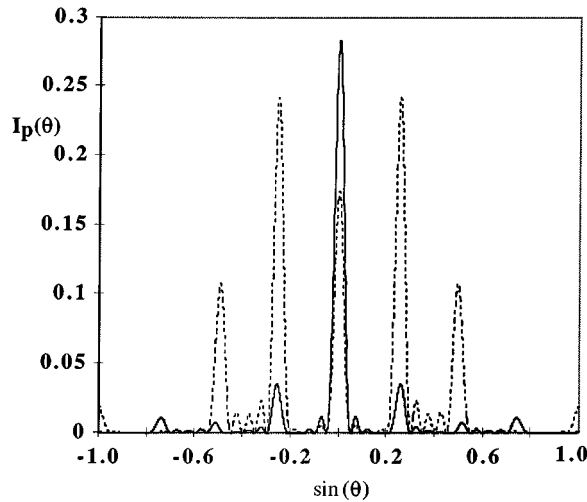


FIG. 8. Fraunhofer diffractions of  $|T(x)|$  (solid curve) and  $\Phi$  (dashed curve) as functions of  $\sin(\theta)$  when  $\Delta_p=2.2$ , and  $I_c=20$ . The other parameters are  $\gamma_{31}=0.1$ ,  $L=4$ ,  $\Delta_c=0$ ,  $\Lambda_{cx}/\lambda_p=4$ , and  $N=5$ .

dispersion in the EIT window, and results in an atomic grating that can effectively diffract light into the first-order diffraction.

This theory is applicable to atomic beams, or atomic cells where the atomic density is so high that collisions become the dominate linewidth-broadening mechanism [3]. This grating may be utilized as a beam splitter for fields whose frequencies are out of reach by the gratings commercially available. Both the direction and the amount of the split light can be controlled by the coupling field. We note that in an atomic beam experiment, the probe diffraction pattern will be shifted if the velocity of the atomic beam changes. As a result, this diffraction pattern may provide insight into not only the internal (atomic energy levels and decay rates) but also the external (velocity) atomic variables.

The phenomenon of EIT in the presence of Doppler broadening is evident from several recent experiments [4]. Although the experimental arrangements for EIG are differ-

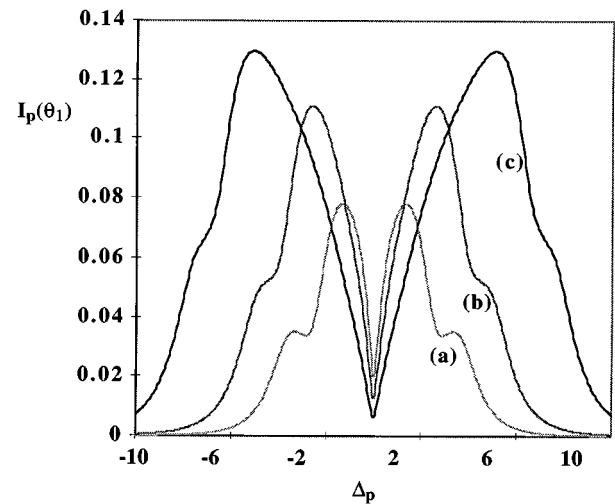


FIG. 9. The first-order diffraction  $I(\theta_1)$  as a function of  $\Delta_p$  when  $I_c =$  (a) 10, (b) 20, and (c) 50. Other parameters are  $\Delta_c=0$ ,  $\gamma_{31}=0.1$ ,  $L=4$ , and  $N=5$ .

ent from those for EIT, the main mechanism leading to EIG is still EIT. As a result, we believe that EIG will be observable in similar experiments, although the diffraction pattern will be less pronounced. In order to extract the main physics, we have assumed that the optical beams are plain waves. In practice, they have a Gaussian profile. Thus our theory applies only to optical beams whose width is much larger than the grating period. When the finite extent of a Gaussian profile is taken into account, the grating efficiency is expected to be reduced. The details of these practical concerns are beyond the scope of this work, and will be left to a future study.

#### ACKNOWLEDGMENTS

The work at the University of Arkansas was partially supported by the Office of Naval Research and the National Science Foundation. The work at Rowan University was supported by a grant from Research Corporation.

- 
- [1] G. Alzetta, A. Gozzini, L. Moi, and G. Orriols, *Nuovo Cimento B* **36**, 5 (1976); G. Alzetta and L. Moi, *ibid.* **52**, 209 (1979).
- [2] H. R. Gray, R. M. Whitley, and C. R. Stroud, Jr., *Opt. Lett.* **3**, 218 (1978).
- [3] K.-J. Boller, A. Imamoglu, and S. E. Harris, *Phys. Rev. Lett.* **66**, 2593 (1991); J. E. Field, K. H. Han, and S. E. Harris, *ibid.* **67**, 3062 (1991); A. Kasapi, Maneesh Jain, G. Y. Yin, and S. E. Harris, *ibid.* **74**, 2447 (1995).
- [4] J. Gea-Banacloche, Y. Q. Li, S. Jin, and M. Xiao, *Phys. Rev. A* **51**, 576 (1995); Y. Q. Li and Min Xiao, *ibid.* **51**, R1754 (1995); M. Xiao, Y. Q. Li, S. Jin, and J. Gea-Banacloche, *Phys. Rev. Lett.* **74**, 666 (1995).
- [5] H. Y. Ling, Y. Q. Li, and M. Xiao, *Phys. Rev. A* **53**, 1014 (1996).
- [6] V. G. Arkhipikin and Tu. I. Heller, *Phys. Lett.* **98A**, 12 (1983).
- [7] O. Kocharovskaya and Ya. I. Khanin, *Pis'ma Zh. Eksp. Teor. Fiz.* **48**, 581 (1988) [*JETP Lett.* **48**, 630 (1988)].
- [8] S. E. Harris, J. E. Field, and A. Imamoglu, *Phys. Rev. Lett.* **64**, 1107 (1990).
- [9] M. O. Scully, S.-Y. Zhu, and A. Gavrielides, *Phys. Rev. Lett.* **62**, 2813 (1989).
- [10] L. M. Narducci, H. M. Doss, P. Ru, M. O. Scully, S. Y. Zhu, and C. Keitel, *Opt. Commun.* **81**, 379 (1991).
- [11] O. Kocharovskaya and P. Mandel, *Phys. Rev. A* **42**, 523 (1990).
- [12] H. Y. Ling, *Phys. Rev. A* **49**, 2827 (1994).
- [13] K. Hakuta, L. Marmet, and B. P. Stoicheff, *Phys. Rev. Lett.* **66**, 596 (1991); G. Z. Zhang, M. Katsuragawa, K. Hakuta, R. I. Thompson, and B. P. Stoicheff, *Phys. Rev. A* **52**, 1584 (1995).
- [14] P. R. Hemmer, D. P. Katz, J. Donoghue, M. Cronin-Golomb, M. S. Shahriar, and P. Kumar, *Opt. Lett.* **20**, 982 (1995).

- [15] Y. Q. Li and M. Xiao, *Opt. Lett.* **21**, 1064 (1996).
- [16] A. Aspect, E. Arimondo, R. Kaiser, N. Vansteenkiste, and C. Cohen-Tannoudji, *Phys. Rev. Lett.* **61**, 826 (1988); *J. Opt. Soc. Am. B* **6**, 2112 (1989).
- [17] F. Papoff, F. Mauri, and E. Arimondo, *J. Opt. Soc. Am. B* **9**, 321 (1992).
- [18] M. R. Doery, R. Gupta, T. Bergeman, and H. Metcalf, *Phys. Rev. A* **51**, 2334 (1995).
- [19] P. Marte, P. Zoller, and J. L. Hall, *Phys. Rev. A* **44**, 4118 (1991).
- [20] L. S. Goldner, C. Gerz, R. J. C. Spreeuw, S. L. Rolston, C. I. Westbrook, W. D. Phillips, P. Marte, and P. Zoller, *Phys. Rev. Lett.* **72**, 997 (1994).
- [21] S. E. Harris, *Phys. Rev. Lett.* **72**, 52 (1994).
- [22] J. H. Eberly, M. L. Pons, and H. R. Haq, *Phys. Rev. Lett.* **72**, 56 (1994).
- [23] R. R. Moseley, S. Shepherd, D. J. Fulton, B. D. Sinclair, and M. H. Dunn, *Phys. Rev. Lett.* **74**, 670 (1995).
- [24] M. Jain, A. J. Merriam, A. Kasapi, G. Y. Yin, and S. H. Harris, *Phys. Rev. Lett.* **75**, 4385 (1995).
- [25] N. Bloembergen and Y. R. Shen, *Phys. Rev.* **133**, A37 (1964).